Development of a Special-Purpose Test Surface Guided by Uncertainty Analysis

T. Wang*
Clemson University, Clemson, South Carolina
and
T. W. Simon†
University of Minnesota, Minneapolis, Minnesota

Development of a recent experimental program to investigate the effects of streamwise curvature on boundary-layer transition required making a bendable, heated, and instrumented test wall, a rather nonconventional surface. The present paper describes this surface, the design choices made in its development, and how uncertainty analysis was used, beginning early in the test program, to make such design choices. Published uncertainty analysis techniques were found to be of great value. Finally, it is shown how the uncertainty analysis was used to determine whether the test surface was qualified for service.

Nomenclature

area = total heating area
C_p = specific heat
C_t = thermocouple calibration constant
k_l = thermal conductivity of lexan (polycarbonate)
k_{in} = thermal conductivity of insulation
k_{ss} = thermal conductivity of stainless steel
PF = power factor
P_d = dynamic pressure
P_s = static pressure (relative to P_{amb})
$\dot{Q}$ = total heater power
$\dot{q}''$ = convective heat flux
RH = relative humidity
R_I = shunt resistance
s = standard deviation
SP = pressure transducer converting factor
St = Stanton number, $=\dot{q}''/\rho_\infty C_p U_\infty (T_w - T_\infty)$
T = mean temperature
T_r = adiabatic temperature
U = streamwise mean velocity
V_L = load voltage drop
V_R = shunt resistor voltage drop
X_i = input parameter
$\bar{X}$ = mean of a sample
ΔX = patch size of which the local Stanton number is representative
δX_i = uncertainty of the parameter X_i
ΔX_i = perturbed value of the parameter X_i
X_R = resultant parameter
ε = emissivity of stainless steel
ρ = density

Subscripts

amb = ambient
c = calibration uncertainty
p = pretest analysis
u = unsteadiness uncertainty
w = wall
1 = first-order analysis.
0 = zeroth-order analysis
∞ = freestream

Received Nov. 16, 1987; presented as Paper 88-0169 at the AIAA 26th Aerospace Sciences Meeting, Reno, NV, Jan. 11–14, 1988; revision received March 16, 1988.

*Assistant Professor, Mechanical Engineering Department. Member AIAA.
†Associate Professor, Mechanical Engineering Department.

Introduction

MEASUREMENTS of convective heat-transfer rates from heated surfaces are now commonplace. However, careful measurements are too few and misconclusions due to incorrect measurement techniques are too frequent. With complexities of surface oxidation, conduction and radiation losses, nonuniformity of material properties, and so forth, final results may have large undocumented errors. Often, an uncertainty analysis is not presented. It is now the view of many that presentation of test results without accompanying uncertainty analysis should not be allowed. It is also the view of some that the uncertainty analyses should begin early in the program and be used to make crucial design choices. In this paper, such a process is exemplified as the design of a unique test surface is presented.

Development of a recent experimental program to investigate the effects of streamwise curvature on boundary-layer transition required making a bendable, heated, and instrumented test wall. Design of such a test surface—one that could be changed from one radius of curvature to another—required rather nonconventional techniques and, therefore, represented some risk. In view of the innovative construction of the test wall and the expectation of large streamwise and spanwise temperature gradients within the region of transition from laminar to turbulent flow, uncertainty analysis was employed to guide the planning of the program. The uncertainty interval is an important published result from the experiment because it shows the best estimate of the interval within which the true value of the result is expected to lie. In doing the analysis, one quickly learns the relative effects of imprecision, unsteadiness, and component uncertainties on the overall uncertainties of the program. One also evaluates the impact on uncertainty of compromises that may be made in favor of flexibility or operating convenience. In this regard, the following study is representative of numerous convective heat-transfer experiments; thus, the important points of this paper can be extrapolated to most experimenters' specific conditions.

Although techniques of uncertainty analysis have been under development, and the uncertainty of experimental data has been presented for several decades, the methodology of uncertainty analysis is still in a state of flux. In fact, although

the importance of uncertainty analysis is being stressed by all, the appropriate methodology is being debated more today than ever before.[1-6] The traditional function of uncertainty analysis has been in reporting the results. More recently, however, authors of the methodology are also discussing how the uncertainty analysis can be used as an aid in the planning of experimental programs.[1,5] This paper will emphasize this aspect by presenting a case where the uncertainty analysis is initiated at the onset of the development of an experimental program and allowed to evolve throughout the entire program. As a base, the uncertainty methodology proposed by Moffat[7] was applied in the present study, although the main ideas of this paper are not restricted to this particular methodology. In addition, a very useful intermediate step, the *pretest* analysis, as labeled herein, was formulated and used as a complement to the existing methodology.

The objectives of this paper are:

1) To document a somewhat novel heat-transfer test section design.

2) To demonstrate the significance and usefulness of uncertainty analysis as an essential tool in *planning*, *developing*, and *controlling* the experiment, as well as in *presenting* the data.

3) To present a thorough uncertainty analysis, including numerical values, of a particular convective heat-transfer study, which should be useful in similar experiments.

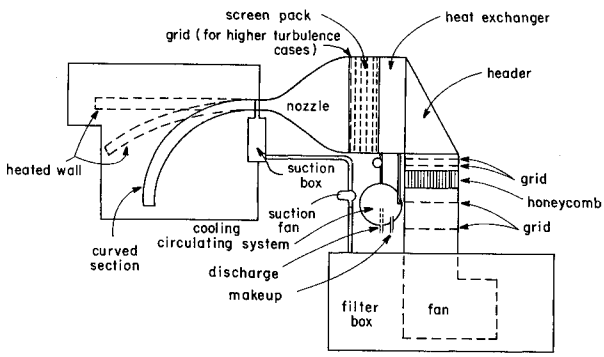

Fig. 1 Curved boundary-layer facility.

4) To introduce a formulation of a pretest analysis (a step that is not traditionally done and has not been introduced previously in detail) and to display its usefulness.

5) To emphasize the importance of *cross-checking* and *closure* using the uncertainty analysis results for qualification of the facility.

Test Program

The test program employs the boundary-layer heat-transfer facility shown in Fig. 1. Air is drawn through filters, forced through a heat exchanger and screen pack, and enters a test region at a nominal velocity of 35 m/s uniform to ± 0.1 m/s, and a temperature of 25°C, uniform to ± 0.05°C. The test region is rectangular, 11.4 × 68.6 cm (4.5 × 27 in.), and is 1.4 m (55 in.) long. One sidewall, 68.6 cm × 1.4 m, is heated to nominally 10°C above the oncoming air temperature with a heat flux of 240 W/m^2, uniform to $\pm 1\%$. The heated wall, a cutaway of which is shown in Fig. 2, was constructed to be flexible so that it could be bent to varying degrees of streamwise curvature. The support wall is a 5-mm (3/16-in.)-thick sheet of polycarbonate plastic (lexan). A 15.24-cm (6-in.)-thick fiberglass insulation pad was installed to minimize backside heat transfer. Adjacent to the lexan support wall is a 1.5-mm (1/16-in.)-thick heating pad constructed of a heater foil circuit sandwiched between glass cloth and silicon rubber sheets. Heating of the wall is effected by Joule heating of this uniformly distributed foil. Bonded to the heater is a 0.25-mm (10-mil)-thick rubber spacer in which 76-μm (3-mil) thermocouple wire is embedded. The thermocouples are well protected and cushioned by the rubber spacer so that they can sustain bending stresses without breaking. They are distributed along the centerline of the test wall with a 2.54-cm (1-in.) spacing and across the span at several streamwise locations. Channels were cut through the rubber spacer in the pattern shown in Fig. 3 to lead the wires to the edges. Covering the thermocouples and in contact with their junctions is a 0.1-mm (4-mil)-thick sheet of stainless steel. This sheet is bonded to the spacer as shown in Fig. 2. The detailed procedures for the composite wall construction were documented in Ref. 8. The freestream temperature was measured with a thermocouple taken from the same manufacturing run as that of the embedded thermocouples. The freestream veloc-

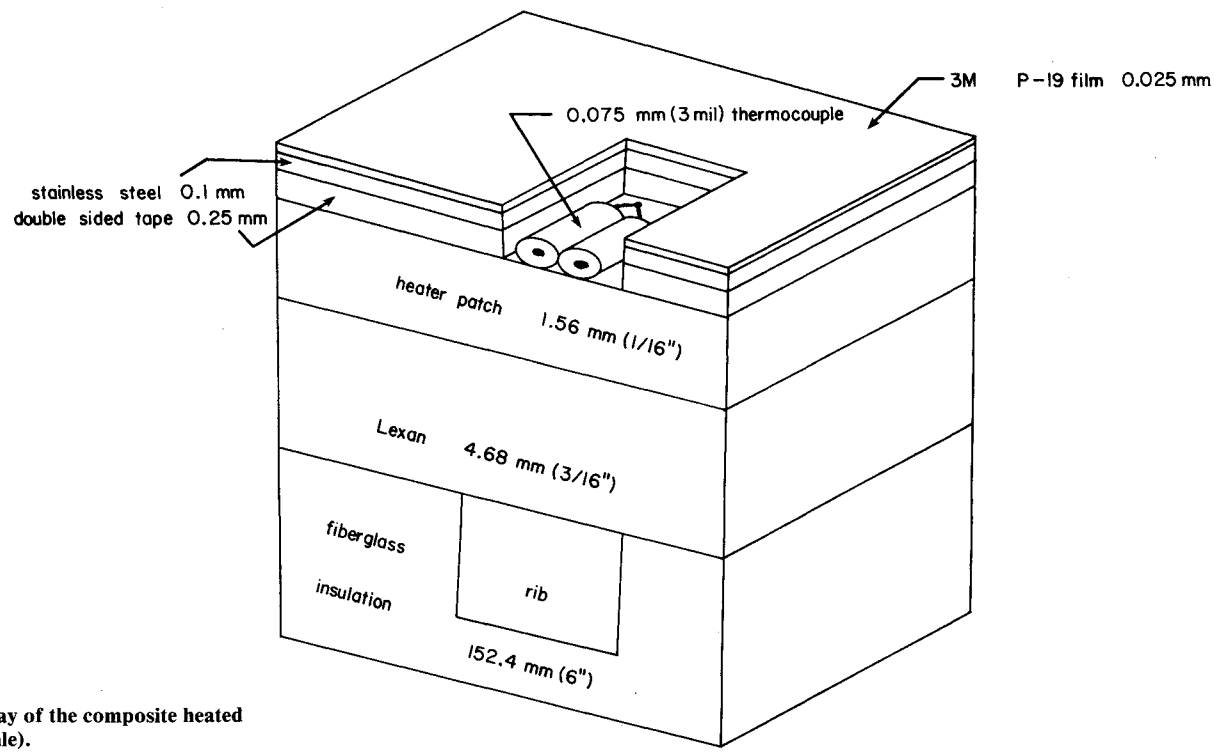

Fig. 2 Cutaway of the composite heated wall (not to scale).

ity was measured using a Pitot tube, wall static ports, and a pressure transducer. The total ac power supplied to the heater, Q, was computed from measured rms values of load voltage, V_L, and series precision resistor voltage, V_R, as $\dot{Q} = V_L V_R / R_I \times$ power factor. The resistance R_I is that of the series precision resistor. The nonuniformity of the heat flux was measured to be within $\pm 1\%$ by a 5×5-cm heat flux meter. The power factor was measured to be within 0.1% of 1.000 over a test period of 24 h. The thermocouple emf values, the pressure transducer output voltage, and the ac voltages, V_L and V_R, were read with a Hewlett-Packard model 3465B digital multimeter.

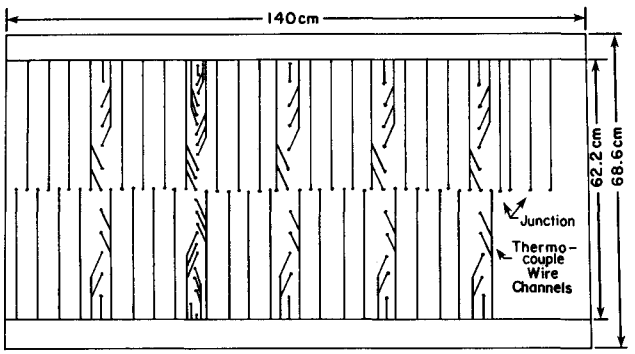

Fig. 3 Layout of the embedded thermocouple channels.

Primary Measure

The expected resultands of the test program is an array of local Stanton numbers, one for each thermocouple location. The Stanton number is computed from the measured data as

$$St = \frac{\dot{q}''_w}{\rho_\infty C_p U_\infty (T_w - T_\infty)}$$

All of the six variables in the preceding equation, except T_w, are dependent variables, which are the resultants of other measurands. For each of these dependent variables, a procedure of backward "tracing" was taken until the root (primary measurand) was found. A simplified block diagram (Fig. 4) illustrates the tracking of each dependent variable. The variables listed outside the dashed box are primary measurands and are considered independent variables. The number of possible independent variables has not been exhausted. Items known to be small were ignored so that the complexity of the presentation could be reduced. For instance, a 10% uncertainty of recovery factor, which contributes only a 0.003°C temperature uncertainty, was not included herein.

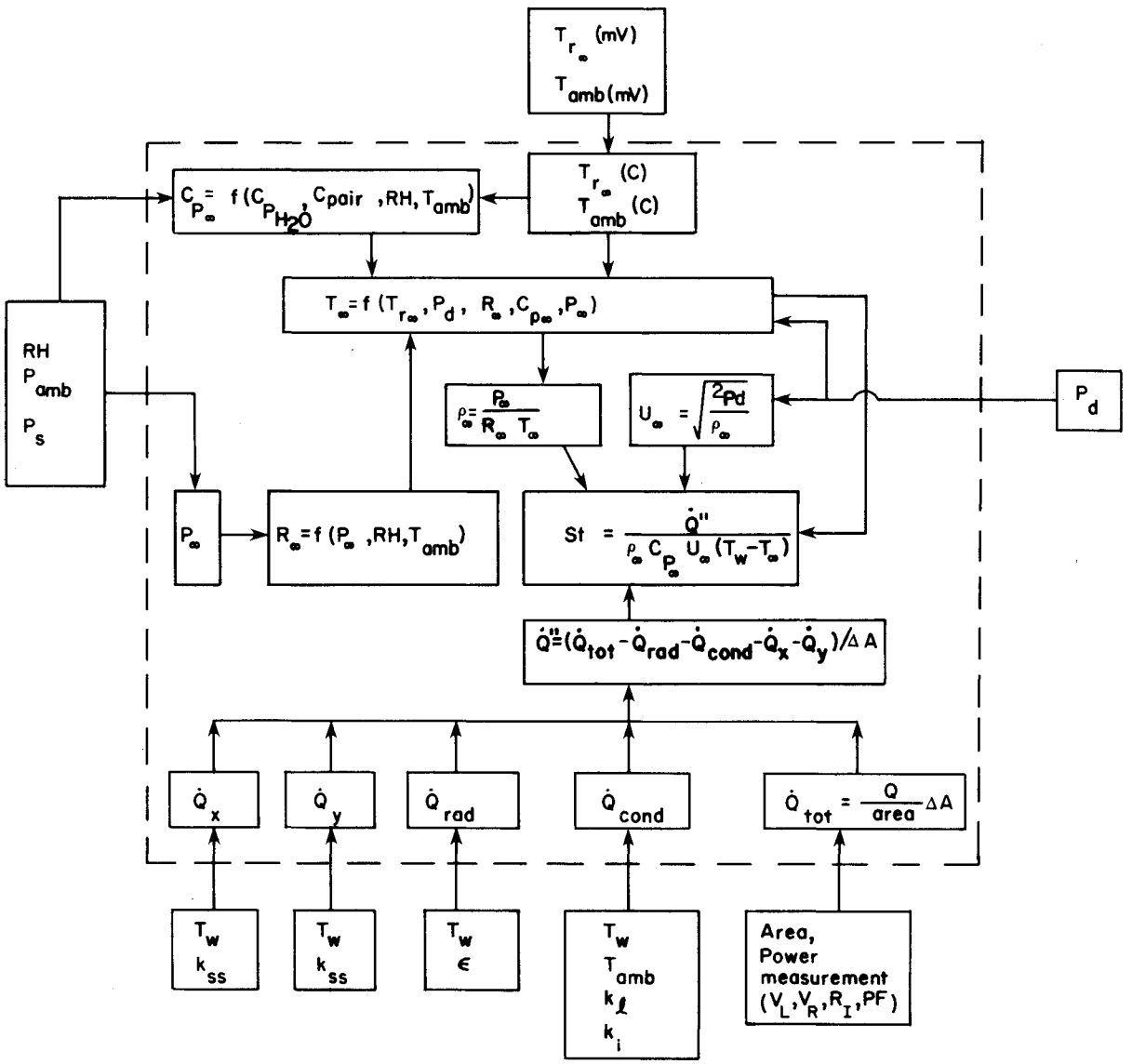

Fig. 4 Simplified block diagram illustrates the backward tracing procedure for identifying the primary measurands. The variables located outside the dashed box are primary measurands.

Uncertainty Analysis

This test program is typical of experiments performed in university laboratories or basic studies in other research facilities. It is one in which a series of single-sample runs is taken, and each run is considered separately. The data are collected through calibrated instruments. The calibration process is one in which a series of readings is taken over a range of the independent variable. All known bias errors are evaluated and removed and a random component for the instrument error can be evaluated from multiple measurements. Associated with the evaluation and removal of the known bias errors is an uncertainty. This is treated like an additional term to the random component of the uncertainty because it is equally probable that the bias error correction is too high as well as too low. This "zero centering" by elimination of all known bias errors is an aspect of the particular methodology chosen herein.[7] Other methodologies require that the known bias errors associated with calibration be evaluated and then used to determine the resultant bias error. The authors have found the chosen methodology more useful, but feel that the important issues of the present paper are not restricted to the methodology chosen. Elimination of known bias errors due to the instruments or other identifiable contributions does not exclude the possibility of bias error entering the experiment by other, unknown, means. Therefore, it is necessary to test for unknown bias error, as will be discussed later. Propagation of random error components (and uncertainties in computed bias error components) was computed using the technique proposed in 1953 by Kline and McClintock.[9] Using this technique, the uncertainties of input parameters to the analysis, δX_i, all based on the same confidence interval, are combined to give a resultant uncertainty, δX_R, of the same confidence interval, using the rms method, as

$$\delta X_R = \left\{ \sum_i \left[\left(\frac{\partial X_R}{\partial X_i} \right) \delta X_i \right]^2 \right\}^{\frac{1}{2}}$$

The technique was also recently recommended in Refs. 10 and 11. The partial derivative term in the preceding equation is the sensitivity of the resultant, X_R, to the parameter X_i. In the present study, it is evaluated in the data reduction program by perturbing each X_i, one at a time. The component uncertainties, δX_i, are evaluated using different guidelines depending on the degree of evolution of the uncertainty analysis, as described by Moffat[7] and discussed below.

Results

The results of the uncertainty analysis vary with the stage of evolution of the analysis or with the level of replication on which the analysis is based.

Zeroth-Order Analysis

The zeroth-order analysis was made in the early stages of the test program design. At this stage, the experiment was in the conceptual design stage and no hardware, specific to this study, existed. Decisions to purchase new equipment, or to use the existing equipment purchased for previous experimentation, were being considered. At this replication level, the only uncertainties recognized were those associated with the interpolation or roundoff error of the proposed recording devices. For this analysis, the uncertainty value, δX_i, associated with each reading, was taken to be one-half of the

Table 1 Input data and results for zeroth and pretest uncertainty analysis

Independent variable	Instrument	Nominal value	Uncertainty of imprecision	Uncertainty of calibration	Zeroth order, %	Pretest, %
P_d (dynamic pressure), V	Voltmeter	1.4600	0.00005	0.0004	0.002	0.014
P_{amb} (ambient pressure), mmHg	Barometer	760.5	0.5	0	0.002	0.002
$T_{r\infty}$ (adiabatic free-stream temperature), mV	Voltmeter	1.495	0.0005	0.0025	0.107	0.534
T_w (wall temperature), mV	Voltmeter	2.047	0.0005	0.0026	0.106	0.553
RH (relative humidity)	Psychometer	0.70	0.005	0.0255	0.005	0.024
T_{amb} (ambient temperature), C	Thermometer	22.8	0.2	0.0125	0.023	0.023
P_s (static pressure), mV	Voltmeter	58.85	0.005	0.02	~0	~0
Area (heating area), m^2	Rule	0.836	2.5×10^{-7}	0	~0	~0
V_L (voltage drop across load), V	Voltmeter	31.62	0.005	0.10	0.020	0.395
V_R (voltage drop across resistor), mV	Voltmeter	31.62	0.005	0.10	0.020	0.395
R_I (shunt resistance for current measurement), Ω	Ohmmeter	0.005	1×10^{-5}	0	0.250	0.250
PF (power factor)		1.000	0.001	0	0.125	0.125
k_l (lexan thermal conductivity), W-m/m^2-C		0.193	0	0.020	0	0.001
k_{in} (insulator thermal conductivity), W-m/m^2-C		0.461	0	0.0067	0	0.255
k_{ss} (stainless steel thermal conductivity), W-m/m^2-C		15.8	0	1.5	0	0.616
ε (stainless steel emissivity		0.55	0	0.08	0	2.401
SP (pressure transducer converting factor), V/m-H_2O	Pressure Transducer	164.95	0	3.299	0	1.002
$\dot{q}''$ (heat flux), W/m^2	Heat flux Meter	239.2	0	2.329	0	1.248
C_t (thermocouple calibration), C	Thermocouple	0.1	0	0.05	0	0.008
Total uncertainty, %					0.32	3.12

Table 2 Stainless steel sheet thickness effect and local *St* representative patch size effect

Sheet thickness effect		Patch size effect	
Thickness of stainless steel, mm	Overall uncertainty in Stanton no., %	Patch size, cm	Overall uncertainty in Stanton no., %
0.05	3.0	0.5 × 0.5	5.8
0.10 (nominal)	3.1	1.0 × 1.0	3.7
0.15	3.3	2.5 × 2.5 (nominal)	3.1
0.20	3.5		

smallest scale division for analog instruments and one-half of the value of an increment of the least significant digit for digital instruments. The quantitative values were usually obtained from the manufacturers' specifications. All calibrations were presumed to be accurate, and the facility and instrumentation were presumed to be steady and free of bias errors. The contributors to the zeroth-order analysis, their nominal values, and their assigned uncertainties are given in Table 1. The table also shows each component's contribution to the resultant Stanton number uncertainty as well as the value of the resultant Stanton number uncertainty. The resultant uncertainty of 0.32% indicates that the proposed instrumentation scheme does not suffer from excessive precision error. If, for example, the precision in reading the thermocouple emf values were considerably poorer, and $\delta St_0/St$ were evaluated to be 10%, the designer of the test program must either consider another instrument or another scheme for measuring temperature. The designer would focus on the measurements that have the largest component contributions. In the present investigation, it was a relief to learn that the proposed scheme for measuring power was sufficiently precise and that an alternate scheme involving, perhaps, a wattmeter, was not necessary. The zeroth-order uncertainty results were used to assist in selecting the instruments based on precision error only.

Pretest Analysis

According to documented methodology (see, for example, Ref. 7), the next analysis in the evolution of the uncertainty analysis would add an uncertainty associated with the unsteadiness of the system to the uncertainty associated with instrument imprecision (discussed earlier). In the methodology proposed by Moffat,[7] this is called the first-order analysis. This analysis cannot be performed, however, until the equipment has been purchased and the experimental facility has been constructed and tested. As the design progressed, it became clear that an intermediate analysis was needed. The "pretest" analysis fills this need. This is the first time that details of a pretest analysis have been given, although Ref. 10 introduces such a step and suggests the components that it would possess. In the pretest analysis, the instrument imprecision uncertainty discussed earlier and labeled the zeroth-order contribution, $\delta X_{i,0}$, was combined with the best estimates of the calibration uncertainties, $\delta X_{i,c}$. These calibration uncertainties included best estimates of uncertainties associated with the removal of known bias errors (calibration and elsewhere in the facility). The pretest uncertainties are given as

$$\delta X_{i,p} = [(\delta X_{i,0})^2 + (\delta X_{i,c})^2]^{\frac{1}{2}}$$

Since, at this stage, actual calibrations had not yet been performed, calibration uncertainties were estimated based on previous experience, including knowledge of the calibration capability of the laboratory. One aspect of this test is that it helps optimize the calibration program and, thus, spares the effort of painstakingly performing an unnecessarily precise calibration or, perhaps, indicates that better calibration facilities must await the completed facility. For example, the time and effort required to perform the calibration for 120 thermocouple junctions with an uncertainty of 0.02°C (1 μV) would be considerably more than the effort to calibrate the same instruments within 0.05°C (2.6 μV). The results of the pretest analysis (Table 1) show that other items (ε, SP, and $\dot{q}''$) contribute more to the resultant uncertainty than does the wall temperature uncertainty, δT_w. Thus, a thermocouple uncertainty of 0.05°C would be satisfactory.

In addition to estimating the calibration uncertainty, models designed to evaluate and correct for known bias errors elsewhere in the facility were incorporated next at this stage of the evolution of the analysis. Because parameters for these models were not precisely known at this stage, they were estimated. Sources of such bias errors (not caused by instruments) in the present study are surface radiation loss, backside conduction loss, and streamwise and spanwise conduction losses. As an example, the correction model for conduction within the stainless steel sheet accounted for a small amount of thermal energy, which conducts through the sheet in the streamwise and spanwise directions. This energy does not contribute to the surface heat flux over the region in which it is claimed that the local Stanton number is representative. The region was considered to be a square, ΔX on each side, centered on the thermocouple junction location. The magnitude of the correction changes with stainless steel sheet thickness, which was considered to be a design variable. It also changes with the size of the patch, ΔX. As the patch size decreases, the uncertainty due to conduction of values that are assignable to that patch increases. For the nominal case, a 0.1-mm-thick stainless steel sheet and a 2.5 × 2.5-cm patch size were chosen. The nominal sheet thickness was thought to be the minimum thickness of steel, which has the rigidity necessary to cover the thermocouples without dimpling. The chosen patch size was based on the thermocouple spacing. As estimates for the analysis, severe streamwise and spanwise temperature gradients of 100°C/m on two adjacent faces of the patch were chosen. This value, thought to be a worst-case representation of the temperature gradient at a patch that is in the vicinity of boundary-layer transition, was taken from Ref. 12. Note that, at this point, the facility did not exist, and, therefore, no experiment had yet been performed. Later, the preceding estimate was replaced with measured values. Based on variations noted in the material property references, the uncertainty assigned to the conductivity of stainless steel was 10% of the nominal value. Table 2 shows how the overall uncertainty on local Stanton number varies with sheet thickness and patch size. The penalty for a thicker stainless sheet is small. Also, Table 2 shows that the reported uncertainty of the local Stanton number must be increased if the size of the patch over which the local Stanton number is claimed to be representative is decreased. It should be emphasized that the graidents imposed are severe for these pretest analyses. Uncertainty analyses formulated after the facility became operational had the benefit of neighboring thermocouple readings from which to calculate the actual gradients.

The correction model for backside heat transfer assumed one-dimensional conduction on the backside, through the polycarbonate support wall and the fiberglass insulation. The thickness of the fiberglass was considered a design variable.

The uncertainty assigned to the conductivity of the polycarbonate sheet was 10% and of the fiberglass was 15% of the nominal values. Table 3 shows the overall uncertainty of local Stanton numbers to be weakly dependent on the insulation thickness. A nominal value of 15 cm was chosen.

The correction model for radiation heat transfer assumed two-body radiation between the test wall at T_w and neighboring walls at temperature T_∞. Gray body behavior was assumed for the test wall and, because the ambient surfaces (mostly plastic) have near-unity values of emissivity at infrared wavelengths, black-body behavior was assumed for the neighboring walls. The nominal value of the stainless steel emissivity was 0.55. A review of the property literature revealed that the uncertainty assigned to this value should be large ($\sim$15%). Table 4 shows that the combination of large emissivity and large uncertainty of emissivity creates an uncomfortably large resultant uncertainty. One possible way to reduce this uncertainty was to use a paint of precisely known emissivity. Table 4 shows that this represents a considerable improvement; although the emissivity was higher and the radiation loss was consequently higher, the uncertainty of the emissivity of this paint was much smaller. Because the wall must be flexible, paint, which was subject to cracking under frequent and severe bending, seemed impractical. Another solution was to cover the surface with a thin reflective film. The film considered was P-19, a 0.025-mm-thick, sun control film manufactured by 3M. The emissivity was given to be 0.30 at 34°C with a 3% uncertainty over a 3-yr life. Table 4 shows that this is a substantial improvement over the bare stainless steel surface. Based on this pretest analysis, it was decided to install the film. Note that, without the uncertainty analysis, the wall emissivity problem might not have been considered, during the design stage, to be an important parameter in this forced convection study. It would have been discovered in later versions of the uncertainty analysis, when there may have been fewer opportunities to correct the problem. The pretest analysis thus proved to be an important intermediate step in the evolution of the uncertainty analysis. With the pretest analysis, hypothetical design configurations were evaluated.

First-Order Analysis

With guidance from the pretest analysis, the facility configuration was fixed and the construction completed. An unsteadiness qualification test of the operating facility was then made as part of the facility qualification. According to the methodology that was chosen for the present study, unsteadiness uncertainty was next added to the instrument imprecision uncertainty in the first-order analysis. Input to the analysis required running the facility until its heat-up was complete, then surveying the time variation of all recorded values. Heat-up required 4 h and was observed as a small drift in surface temperature. Its rate was impeded by the slow development of the temperature profile in the backside insulation. Unsteadiness readings were then taken over a period of 1 h. Twenty readings were recorded for each parameter. (Long-period unsteadiness was neglected after a dozen tests, conducted within a six-month period, showed that the short-period unsteady fluctuations were considerably smaller than were the long-period unsteady fluctuations.) These were input into the uncertainty analysis. The s was calculated, and the uncertainty due to unsteadiness, $\delta X_{i,u}$, taken to be twice the standard deviation, was computed for each contributor. These were incorporated into the analysis by using the rms method, giving each variable's first-order uncertainty contribution as

$$\delta X_{i,1} = [(\delta X_{i,0})^2 + (\delta X_{i,u})^2]^{\frac{1}{2}}$$

Input to, and results of, the first-order analysis are shown in Table 5. Note that unsteadiness has increased the total uncertainty from 0.32% in the zeroth-order analysis to 2.6%. This is a significant increase but is not alarming because the total uncertainty is still small. A review of Table 5 shows that the only significant unsteadiness contribution is in the wall temperature measurement. It is felt that this is because of the inherent unsteadiness of boundary-layer flow in the vicinity of transition from laminar to turbulent flow.

In 20 repeated trials over a period of 1 h (after a sufficient heat-up time), readings were taken and Stanton numbers were calculated—one value for each trial. The rms deviation of these Stanton number values was found to be 1.6%. Two times this rms deviation is approximately equal to the first-order uncertainty, δSt_1. This indicates that there are no significant contributors to uncertainty that are not "recorded" in the data reduction program. Because of this closure and a sufficiently small first-order uncertainty, it was decided that unsteadiness was not a problem and that the test program could continue.

*N*th-Order Analysis

The next analysis in the evolution, called by some the *N*th-order analysis, includes uncertainties caused by imprecision, unsteadiness, calibration error, and errors in the correction models incorporated to minimize all known bias errors. It combines the first-order analysis with the calibration and modeling uncertainties discussed in the pretest analysis, but now updated to include measured input

$$\delta X_{i,n} = [(\delta X_{i,0})^2 + (\delta X_{i,u})^2 + \delta(X_{i,c})^2]^{\frac{1}{2}}$$

This analysis is based on the final design configuration and the most up-to-date nominal values of the input parameters.

Table 3 Backside heat-transfer effect

Thickness of fiberglass, cm	Back loss, %	Total Stanton no. uncertainty, %
5.0	4.3	3.31
10.0	2.1	3.16
15.2 (nominal)	1.4	3.12
20.0	1.1	3.11

Table 4 Effect of radiation

	Emissivity	Radiation loss, %	Uncertainty of emissivity, %	Overall uncertainty on Stanton no., %
Bare stainless	0.55	13	10	2.5
sheet	0.55	13	15	3.1
	0.55	13	20	3.6
Solar collector				
black paint	0.95	23	1	2.2
3M reflective film	0.30	7	3	1.9

It has the benefit of actual measurements and calibrations to replace estimated values, e.g., the stainless steel sheet conduction model used the measured temperature gradient of 20°C/m in place of the worst-case estimated gradient of 100°C/m, which was used in the pretest analysis. Because the estimated thermocouple calibration uncertainty of 0.05°C, used in the pretest analysis, did not represent a large contribution to the overall uncertainty, that value was used in the Nth-order analysis and the calibration was done with sufficient care to achieve this uncertainty. Input to, and results of, the Nth analysis are shown in Table 5. The uncertainty of the wall temperature measurement, due to unsteadiness, remains the largest contributor. This could be reduced by averaging n values from repeated trials over an appropriately long time. The unsteadiness uncertainty term would then be reduced to $1/\sqrt{n}$ times the single-sample value. Because the single-sample Nth-order uncertainty was satisfactorily small (3.0%), averaging was considered unnecessary.

Closure

The Nth-order uncertainty represents the best guess of the range about the measured value in which the true value is expected to lie, with 20 : 1 odds. This presumes that all sources of significant bias error have been included. There is a possibility that significant unidentified bias errors may exist, however. Therefore, the experimental results must be compared to physical laws and results of other identical experiments that are recognized to be correct. This final cross-checking and closing procedure is very important and, unfortunately, is frequently ignored. An unsatisfactory comparison would indicate an oversight in the uncertainty analysis; either a signficant bias error was not incorporated or an input to the uncertainty analysis was too optimistic. The uncertainty analysis comparison is satisfactory when the check (comparison with a previous case or with a physical law) balances to within δSt_N. When satisfactory closure is achieved, the uncertainty analysis results assume their ultimate function of presenting the experimentor's best estimate of the inaccuracy of the data—the traditional use of the uncertainty analysis.

In the present experiment, the tunnel was first put in a straight-wall configuration. Then, an all-laminar flow case and a transitional flow case, each with a low freestream turbulence intensity (0.3 and 0.68%, respectively), were performed. However, a lack of energy balance (11 and 15%, respectively) was found in both cases as the result of the lack of two-dimensionality in the flow over portions of downstream laminar regions of both cases and in the transitional region for the transitional case. This three-dimensionality was due to an earlier transition near the endwalls. Since this effect was not observed until the most downstream portion of the all-laminar case, this case was still expected to display the proper relationship of Stanton number vs Re_x, and was thus used as one check of data accuracy. The comparison with a laminar correlation taken from Ref. 15 is shown in Fig. 5. As can be seen, the comparison is good for the upstream portion of the plate. Agreement was found to within 5%. The 5% difference is satisfactory in that a 3.08% uncertainty claimed by the uncertainty analysis and an uncertainty band of at least 2% is expected for the correlation.

Because of the three-dimensionality in the downstream portion of the laminar flow and in the transitional flow for these two cases, neither was chosen for an energy balance qualification test. A higher free stream turbulence case (2%) was performed. In this case, two-dimensionality was verified

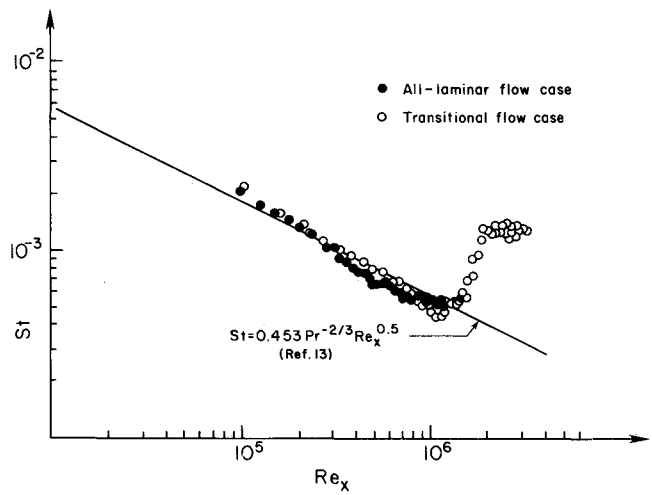

Fig. 5 Stanton number vs Reynolds number for two experimental tests.

Table 5 First and Nth-order uncertainty analysis

Independent variable	Nominal value	Uncertainty of imprecision	Uncertainty of unsteadiness	Uncertainty of calibration	First order		Nth order	
					Uncertainty magnitude	Individual uncertainty, %	Uncertainty magnitude	Individual uncertainty, %
P_d,	1.4600	0.00005	0.0040	0.0004	0.0040	0.176	0.0040	0.176
P_{amb}, mmHg	745.5	0.5	5.0	0	5.0	0.332	5.02	0.332
$T_{r\infty}$, mV	1.495	0.0005	0.0045	0.0025	0.00453	0.901	0.00517	1.028
T_w, mV	2.047	0.0005	0.010	0.0026	0.010	2.359	0.010	2.359
RH	0.70	0.005	0.10	0.0255	0.10	0.097	0.10	0.097
T_{amb}, C	22.8	0.2	1.5	0.0125	1.51	0.149	1.51	0.149
P_s, mV	214.20	0.005	4.00	0.02	4.00	~0	4.00	~0
Area, m^2	0.836	2.5×10^{-7}	0	0	2.5×10^{-7}	~0	2.5×10^{-7}	~0
V_L, V	31.62	0.005	0.05	0.10	0.05	0.175	0.112	0.392
V_R, mV	31.62	0.005	0.02	0.10	0.021	0.007	0.102	0.357
R_l, Ω	0.005	1×10^{-5}	0	0	1×10^{-5}	0.221	1×10^{-5}	0.221
PF	1.000	0.001	0	0	0.001	0.111	0.001	0.111
k_1, W-m/m^2-C	0.193	0	0	0.020	0	0	0.020	0.001
k_{in}, W-m/m^2-C	0.461	0	0	0.0067	0	0	0.0067	0.227
k_{ss}, W-m/m^2-C	15.8	0	0	1.5	0	0	1.5	0.109
ε	0.30	0	0	0.01	0	0	0.01	0.265
SP, V/m-H_2O	164.95	0	0	3.299	0	0	3.299	1.000
$\dot{q}''$, W/m^2	239.2	0	0	2.329	0	0	2.392	1.107
C_l, C	0.1	0	0	0.05	0	0	0.05	0.002
Total uncertainty, %						2.58		3.08

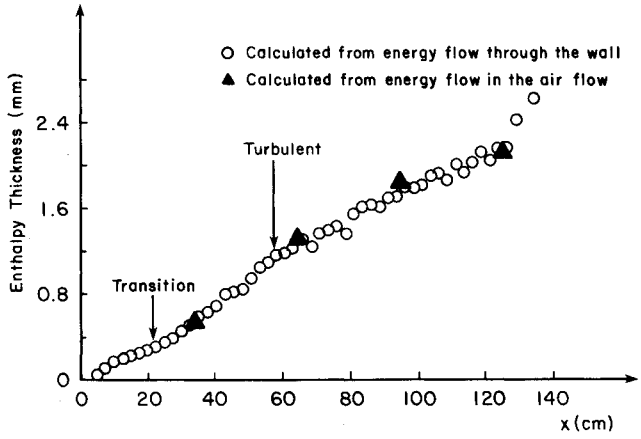

Fig. 6 Energy balance for higher freestream turbulence (2%) case.

with the embedded thermocouples[13] and two-dimensional energy balance techniques for qualifying the facility were available. Balances between the energy flow through the wall and the increase in energy in the airflow, taken at five streamwise locations on the centerline, are shown in Fig. 6. The lack of energy closure is only 5%.

Having found satisfactory agreement, the curved-wall cases, for which the facility was designed, were run. Prior to each new series of curved-wall tests, successful energy balances were made.

Conclusions

Development of a flexible, uniformly heated, composite wall for a recent series of experiments was guided by the uncertainty analysis. Design choices and compromises were necessary because of the requirement that the wall be bendable. The uncertainty analysis proved extremely useful in making important design choices. The following summarizes the important conclusions:

1) The zeroth-order analysis confirmed that the chosen instrumentation was sufficiently precise.

2) The pretest analysis was found to be useful for testing design concepts and determining satisfactory configurations while in the early planning stage. It aided in the facility design by confirming the chosen stainless steel sheet and fiberglass insulation thicknesses and by identifying the largest uncertainty contributor to be the stainless steel surface emissivity; this was an unexpected result. It also aided in evaluating the tradeoffs between the stated local uncertainty and the size of the region over which the local Stanton number could be considered representative.

3) The first-order analysis showed that unsteadiness effects are significant, but not excessive. Averaging repeated-case readings would decrease the first-order uncertainty, but this was considered unnecessary.

4) The Nth-order analysis gave estimated bounds on the error in the measurements. Its results showed the allowable disagreement between present measurements and accepted data and correlations in the literature under baseline conditions. It was also used for checks of energy balance closure. The Nth-order results were presented with the reported measurements.

5) The final closure and cross-checking using the uncertainty analysis were emphasized to be a necessary procedure for identifying unknown but significant bias errors.

The bendable, uniformly heated, multilayered test wall has proven to be successful in later curved flow studies.[8,13,14]

Acknowledgments

This study was partially supported by NASA Lewis Research Center Grant NAG 3-286. The grant monitor is Dr. Raymond Gaugler. Additional support was provided by the Graduate School of the University of Minnesota and the South Carolina Energy Research and Development Center.

References

[1]Kline, S. J., "The Purposes of Uncertainty Analysis," *ASME Journal of Fluids Engineering*, Vol. 107, June 1985, pp. 153–160.

[2]Lassahn, G. D., "Uncertainty Definition," *ASME Journal of Fluids Engineering*, Vol. 107, June 1985, p. 179.

[3]Heidrick, T., "Discussion of Symposium on Uncertainty Analysis," *ASME Journal of Fluids Engineering*, Vol. 107, June 1985, p. 180.

[4]Kline, S. J., "1983 Symposium on Uncertainty Analysis Closure," *ASME Journal of Fluids Engineering*, Vol. 107, June 1985, pp. 181–182.

[5]Moffat, R. J., "Using Uncertainty Analysis in the Planning of an Experiment," *ASME Journal of Fluids Engineering*, Vol. 107, June 1985, pp. 173–178.

[6]Coleman, H. W. and Steele, W. G., "Some Considerations in the Propagation of Bias and Precision Errors into an Experimental Result," American Society of Mechanical Engineers Paper FED Vol. 58, 1987.

[7]Moffat, R. J., "Contributions to the Theory of Single-Sample Uncertainty Analysis," *ASME Journal of Fluids Engineering*, Vol. 104, June 1982, pp. 250–260.

[8]Wang, T., "An Experimental Investigation of Curvature and Freestream Turbulence Effects on Heat Transfer and Fluid Mechanics in Transitional Boundary Layer Flows," Ph.D. Dissertation, Mechanical Engineering Dept., Univ. of Minnesota, Minneapolis, MN, Dec. 1984.

[9]Kline, S. J. and McClintock, F. A., "Describing Uncertainties in Single-Sample Experiments," *Mechanical Engineering*, Jan. 1953, pp. 3–8.

[10]*Measurement Uncertainty—Instruments and Apparatus*, ANSI/ASME Performance Test Code 19.1- 1985, April 1986.

[11]Abernathy, R. B., Benedict, R. P., and Dowdell, R. B., "ASME Measurement Uncertainty," American Society of Mechanical Engineers Paper 83-WA/FM-3, Nov. 1983.

[12]Simon, T. W. and Moffat, R. J., "Turbulent Boundary Layer Heat Transfer Experiments: Convex Curvature Effects Study on a Convexly Curved Wall," *Heat Transfer*, Vol. 105, Nov. 1983, pp. 835–840.

[13]Wang, T., Simon, T. W., and Buddhavarapu, J., "Heat Transfer and Fluid Mechanics Measurements in Transitional Boundary Layer Flows," *ASME Journal of Engineering for Gas Turbine and Power*, Vol. 107, Oct. 1985, pp. 1007–1015.

[14]Wang, T. and Simon, T. W., "Heat Transfer and Fluid Mechanics Measurements in Transitional Boundary Layers on Convex-Curved Surfaces," *ASME Journal of Turbomachinery*, Vol. 109, July 1987, pp. 443–452.

[15]Kays, W. M. and Crawford, M. E., *Convective Heat and Mass Transfer*, 2nd ed., McGraw-Hill, New York, 1980.